



Universität Hamburg

DER FORSCHUNG | DER LEHRE | DER BILDUNG

Bachelor Thesis

Signal Evolution along the Length of a Straw Tube Detector

Institut für Experimentalphysik
Universität Hamburg

Sofia Brozzo

Matr.-Nr. 6927266

First supervisor: Dr. Daniel Bick

Second supervisor: Prof. Caren Hagner

January 2021

Abstract

For the Search for Hidden Particles (SHiP) experiment planned at CERN, the Straw Tube detector is to be characterized. SHiP is intended to be a background minimizing particle detector which is supposed to be able to discover new, rarely interacting particles. A prototype of the straw tube detector was studied for the purpose of determining a evolution of the amplitude of the electric signal. In order to achieve signals that are as comparable as possible, it is important to know all the parameters that can influence the signal shape. For this purpose, the signal evolution was investigated dependent on the distance travelled by the signal in the wire of the straw tube. The signal amplitude was investigated for different ionization sources and operating voltages.

Zusammenfassung

Für das am CERN geplante SHiP-Experiment (kurz für Search for Hidden Particles) soll der Straw Tube Detektor charakterisiert werden. SHiP fokussiert sich auf die Suche nach neuen, minimal interagierenden Teilchen, wofür ein minimaler Untergrund essentiell ist. Ein Straw-Tube-Prototyp wurde untersucht, um die Entwicklung der Amplitude des elektrischen Signals zu ermitteln. Um möglichst vergleichbare Signale zu erreichen, ist es wichtig, alle Parameter, die die Signalform verändern können, zu kennen. Es wurde dafür die Signalentwicklung in Abhängigkeit von der Strecke, welche das Signal im Draht der Straw Tube zurücklegt, untersucht. Die Signalthöhe wurde für verschiedene Ionisationsquellen und Betriebsspannungen untersucht.

Contents

1	Introduction	5
2	Theoretical Background	7
2.1	The Standard Model	7
2.2	Physics beyond the Standard Model	9
3	The SHiP Experiment	11
3.1	Motivation	11
3.2	Detector Setup	12
4	Drift Tubes	15
4.1	Working Principle	16
4.2	Trigger	16
4.3	Gas Ionization	17
4.4	Electric Field	19
4.5	Drift Gas	20
4.6	Gas Gain	21
4.7	Signal Characteristics	21
5	Experimental Setup	23
5.1	Straw Tubes	23
5.2	Signal Sources	24
5.3	Trigger Setup	25
5.4	Gas System	26
5.5	Electronics	27

6	Measurements and Analysis	29
6.1	Signal Characterization using Atmospheric Muons	29
6.1.1	Muon Signals	30
6.1.2	Drift Time	31
6.1.3	Muon Signal Evolution	32
6.2	Signal Characterization using Gamma Rays	36
6.2.1	Gamma Signals	37
6.2.2	Gamma Signal Evolution	37
6.2.3	Discussion	39
7	Summary and Outlook	43
	List of Figures	45
	Bibliography	47
A	Additional Figures	51

Chapter 1

Introduction

The Standard Model is considered a key element of particle physics. However, certain phenomena like the neutrino oscillation and Dark Matter cannot be described by the Standard Model. To explain these phenomena, a look outside the Standard Model is needed. The planned Search for Hidden Particles (SHiP) experiment at CERN offers the option to find still unknown, rarely interacting particles, such as the heavy neutral lepton (HNL). In addition SHiP will make the first direct detection of the anti-tau neutrino possible. The experiment uses the 400 GeV energy proton beam of the Super Proton Synchrotron (SPS). In order to detect rarely interacting particles, it requires a minimal background. One detector used in SHiP is the Spectrometer Straw Tracker (SST), which is designed for track and vertex reconstruction of charged particles. The SST will be located at the end of a vacuum vessel in which decays of unknown particles could be observed. The SST contains a large number of thin drift tubes, the so-called straws.

Drift tubes are a frequently used component of particle detection. They consist of a conductive tube filled with a suitable gas mixture. A wire is placed in its center. A particle passing through the tube leads to the ionization of the gas. An applied potential between the wire as anode and the tube wall as cathode causes the ions and electrons to drift along the electric field lines. A signal pulse can be measured when the electrons reach the anode wire.

Before setting up the experiment, it is important to know the properties of the straws. For this purpose a prototype, using four of these straws, was built. In this thesis the signal amplitude was examined depending on the position at which the particle passes through

the straw detector. For this purpose, two different ionization sources, atmospheric muons and gamma rays from an Fe-55 source, were used. The signal intensity was measured at different positions along the straws. An increase of the signal amplitude was observed for an increase in the distance the signal has to travel. In this thesis first in chapter 2 the basics of particle physics, the standard model and physics beyond the standard model are discussed. In chapter 3, the SHiP experiment is motivated and presented in more detail. The physics of drift tubes is then discussed in the following chapter 4, followed by a description of the experimental setup in chapter 5. The measurements are evaluated and discussed in chapter 6. Finally, the summary, as well as an outlook is in chapter 7.

Chapter 2

Theoretical Background

2.1 The Standard Model

The Standard Model of particle physics was proposed as an attempt to unify all physical interactions. It includes three of the four fundamental forces and can confidently explain almost all known physical phenomena [1]. Figure 2.1 visualizes all known elementary particles, their antiparticles and the gauge bosons of the Standard Model. They are considered elementary because it is assumed that they have no inner structure. The gauge bosons are exchange particles describing the interactions between particles. The elementary particles all have a spin of $1/2$ making them fermions. The gauge bosons all have a spin of 1 . The fermions can be separated into six flavors each of quarks and leptons and can further be divided into three generations. The lightest, most stable, first generation is most present in our environment. It consists of up and down quark, the foundation of atomic nuclei, as well as electron and electron neutrino. The second and third generation are increasingly more unstable, therefore their appearance in our environment is rare.

The three fundamental forces described by the Standard Model are the weak force, transmitted by the W^\pm - and Z^0 -boson, the strong force via gluons and the electromagnetic force via photons. The fourth force, which is not included in the Standard Model is gravity. The six quarks (u, d, c, s, t, b) each carry a color charge (red, blue, green) which can be exchanged by a gluon. Antiquarks carry the respective anticolor. Gluons themselves are the only other particles holding color charges. Therefore the strong interaction is unique to quarks making them the only particles influenced by all fundamental forces. Aside from the color charge quarks have a specific electric charge of $2/3$ (u, c, t) or $-1/3$ (d, s, b) with

antiquarks having the inverted charge.

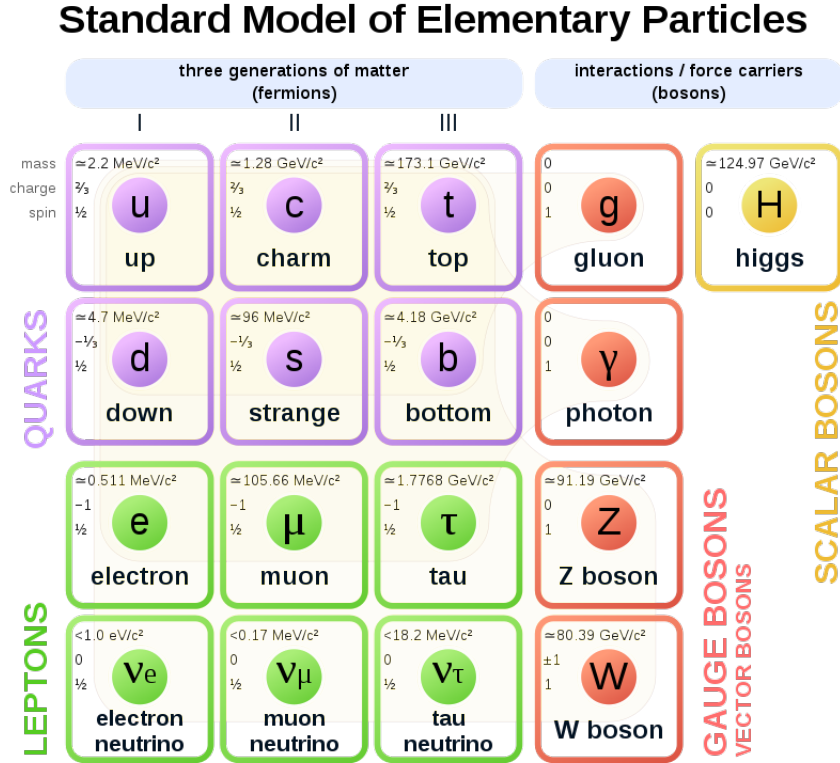


Figure 2.1: The Standard Model of particle physics [2]. Here the six quarks are visualised in purple, the leptons are green, the gauge bosons in red and the higgs in yellow.

Leptons are categorized into electrically charged leptons e , μ , τ with each their own electrically neutral neutrino ν_e , ν_μ and ν_τ . While the charged leptons have an accurately determined mass, within the Standard Model neutrinos were for a long time assumed to be massless. The Homestake experiment in 1968 [3] was the first experiment to discover the solar neutrino problem. This resulted in the proposal of a mechanism called neutrino oscillation, which has been verified in several experiments, first in 1998 by the Super-Kamiokande experiment [4]. This implies that neutrinos must have a mass. At least an upper mass limit has been included in the description of neutrinos in the Standard Model.

The electromagnetic force interacts with electrically charged particles, which include all fermions of the Standard Model with the exception of neutrinos. Photons have no mass and in vacuum an infinite range. The weak force is the only fundamental interaction of

the Standard Model interacting with all fermions. The weak force even allows quarks to change their flavors. Additionally the weak force is special in that the exchange bosons W^{\pm} - and Z^0 are the only gauge bosons with mass. This mass causes the W^{\pm} - and Z^0 bosons to be considered weak. While the weak force's coupling constant is in the same order of magnitude as the coupling constant for the electromagnetic force, the propagator depends antiproportionally on the mass of the boson. This results in couplings being less likely. The gauge bosons of the weak interaction only couple with left-handed particles, or right-handed antiparticles.

The latest addition to the Standard Model is the higgs boson which was discovered 2012 at CERN [5][6]. It was first introduced as a means of explaining the mass of the W^{\pm} - and Z^0 -boson. The higgs boson is not a gauge boson but a scalar boson and the only particle of the Standard Model with a spin of 0 .

2.2 Physics beyond the Standard Model

The Standard Model describes many physical phenomena accurately, however, there are some which cannot be described by the Standard Model at all. One of these phenomena is gravity, which is considered the fourth of the fundamental forces. For it there is no exchange particle in the standard model. Another phenomenon is the baryon asymmetry. It states that in the visible part of the universe there is huge disparity between observed baryonic and antibaryonic matter meaning there are more particles than antiparticles. One part of the explanation could come from the CP violation [7] of the weak interaction which in itself is unexplained. The charge conjugation parity symmetry states that all particles should behave identically if mirrored. While this is the case for the electromagnetic and strong interaction, the weak interaction couples only with left-handed particles. Another topic of research in this area are neutrino oscillations that are already mentioned in section 2.1. Within the Standard Model neutrinos are assumed to have no mass. However, a flavor oscillation can be detected for neutrinos which is currently explained by the fact that the lepton flavor eigenstate of a neutrino is actually a superposition of three mass eigenstates.

To explain these phenomena one has to look beyond the Standard Model for new particles. There are different approaches to find these particles. With the assumption that there could be particles heavier than those already found, one would need to upgrade cur-

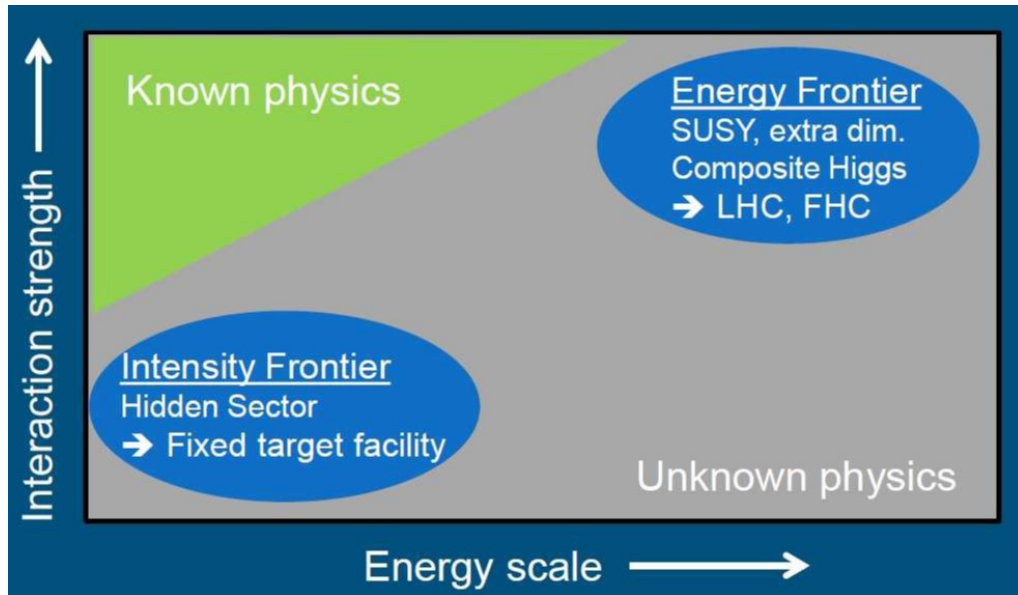


Figure 2.2: Possible areas to search for new particles [8]. The main focus of the search is on the energy frontier and the intensity frontier depending on the interaction strength and the rest energy of the particle.

rent accelerators to reach higher energy levels in order to create them. This approach is called the energy frontier. There could also exist particles that are very weakly interacting and therefore simply not visible to us. To detect these possibly rare interactions high statistics are necessary, therefore this approach is called the intensity frontier. Both are visualized in figure 2.2.

Chapter 3

The SHiP Experiment

3.1 Motivation

SHiP is a planned fixed-target experiment at CERN. SHiP is designed to produce many exotic particles with the aim to search for new particles in a low energy and weak interaction range. New potential particles have been proposed in an attempt to expand the Standard Model. One suggestion for such a particle that could be detected by SHiP is the heavy neutral lepton (HNL) [9]. The HNL is a benchmark model of SHiP and in theory could explain several inconsistencies at once [10]. HNLs could explain the baryon asymmetry [11], their low interaction making them ideal Dark Matter candidates and a coupling of HNLs and neutrinos could be an explanation of the small neutrino masses. HNLs would be the right-handed partners to the left-handed neutrinos. As the name suggests such a particle is expected to be massive but carry no charge. The idea of HNLs as right-handed neutrino partners is based on the seesaw mechanism [12]. It states that the mass of the left handed neutrinos is dependent on the mass of the right-handed ones. With an increased mass of those, the mass of the left-handed neutrinos decreases. Other particles that SHiP can search for are dark photons, dark scalars and axion-like particles. For these particles, models of their possible interactions with known matter already exist, which can be searched for in SHiP.

A dedicated detector also gives the opportunity to study ν_τ and $\bar{\nu}_\tau$ more extensively. This is of importance because while ν_e and ν_μ have been studied in a high number of experiments, the ν_τ has not. SHiP will presumably also be the first experiment observing $\bar{\nu}_\tau$. To create a high number of tau neutrinos, the target material is specifically chosen to

create charmed mesons. These are ideal to produce $\bar{\nu}_\tau$ because of their high mass and their likeliness to decay leptonically.

3.2 Detector Setup

The experiment is intended to be at the proposed Beam Dump facility to use the beam of the Super Proton Synchrotron (SPS), an accelerator with a circumference of 6.9 km. The beam will have a high intensity of $4 \cdot 10^{13}$ protons per spill and an energy of approximately 400 GeV. A spill is an extraction of protons over a time span of one second. It is directed onto a dense proton target, made as a hybrid of titanium-zirconium doped molybdenum and pure tungsten. The whole setup for the experiment is visualized in figure 3.1. The high intensity of the beam heats the target, meaning water cooling is required to keep the target temperature stable. This specific combination of materials was chosen in order to produce a high number of heavy mesons while minimizing the production of muons and neutrinos. The muon and neutrino background is reduced by the short nuclear interaction length of the target. In general the background reduction to an absolute minimum is necessary for an experiment like SHiP. The hadrons are stopped by a hadron absorber directly after the target and the muons are additionally filtered by an active muon shield diverting the muons to the sides via a magnetic field. With this set up, it is possible to reduce the muon background by six orders of magnitude. The SHiP experiment uses several detectors to fully reconstruct the events. Directly after the muon shield the scattering and neutrino detector (SND) is positioned. It consists of an emulsion target combined with tracker planes and a downstream tracker. All this is located in a 1.2 T horizontal magnetic field [13]. Tau neutrinos can be detected by their interaction with the neutrino target where τ leptons are then produced. Tau leptons have a short lifetime of $2.903 \cdot 10^{-13}$ s [14] and afterwards decay mostly hadronic. To determine whether a ν_τ or a $\bar{\nu}_\tau$ was observed, the charge of the τ lepton and its decay products can be measured. This is realized by the spectrometer which record the tracks of the decay products. The SND is planned to be used not only for neutrino physics but also for the search of light dark matter scattering [15].

After the SND the Hidden Sector (HS) decay volume as well as the HS decay spectrometer follow. The aim is to observe as many decays as possible in the volume and to search for expected decays that indicate new particles. The HS decay volume is run with a pressure of 10^{-2} bar [15] to further minimize the background. This is due to inelastic neutrino scatter-

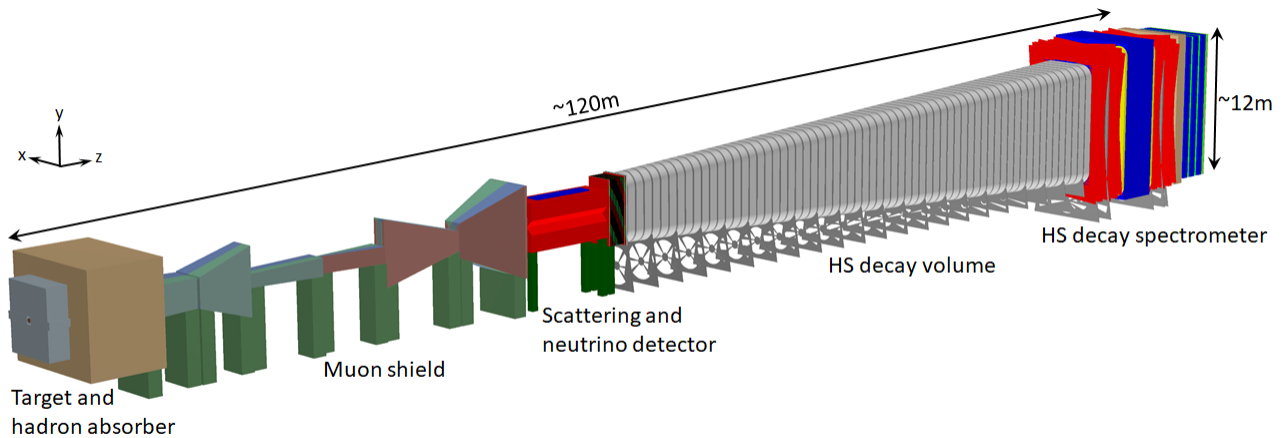


Figure 3.1: The SHiP detector. The beam is oriented in z-direction and hits the target on the left. The following hadron absorber and muon shield minimize the background. The neutrino detector is placed next, followed by the hidden sector detector [13].

ing with air molecules. It is surrounded by a Surround Background Tagger system, which ensures that the signals come from within the vessel and not from outside background. A timing detector outside the vacuum vessel is used as a further background reduction. An electromagnetic calorimeter is used as well as the spectrometer that directly follows the vacuum vessel. This spectrometer consists of a dipole magnet and four tracking stations, each including four views which measure in y-direction (compare figure 3.1) and at an angle of $\pm 5^\circ$ to it. Each of them contains 14 to 15 modules which have 32 tubes in two layers. This results in a total number of approximately 16 000 straw tubes. These thin drift tubes were the subject of this thesis and are further described in the next chapter 4, as well as 5.1.

Chapter 4

Drift Tubes

The focus of this thesis will be the characterization of drift tubes therefore a detailed discussion of their working principle is necessary. A drift tube is a detector commonly used to track high energy particles. Drift tubes are for example used in collider and fixed-target experiments where they are used for track reconstruction. This is done by the addition of a magnetic field.

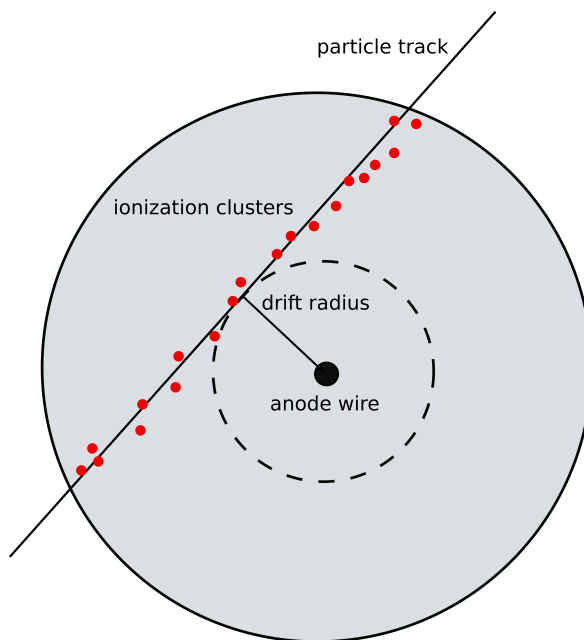


Figure 4.1: Cross section of a drift tube. The tube is filled with a gas mixture, visualized in grey. A passing particle results in the red ionization clusters along the track. The drift radius describes the shortest distance from track to wire and is marked by the dashed line.

4.1 Working Principle

Figure 4.1 illustrates the working principle of such a detector. The center piece is a wire which is placed in the middle of a conductive tube filled with electrically neutral drift gas. A high voltage (HV) is applied between wire and tube so that if the gas is ionized, the resulting ion and electron are both affected by the radially symmetric electric field and drift towards cathode or anode depending on their charge. Because of their smaller rest mass, the electrons reach the wire faster than the ions reach the cathode. Along their paths, the particles are accelerated by the voltage and if they gain enough kinetic energy, they can further ionize particles resulting in larger signals. The signal of the electrons is recorded and used for the characterization. The electrons reaching the wire first are the ones with the shortest distance. In figure 4.1 this shortest distance is visualized as the drift radius. These electrons on the drift radius take a specific time to reach the wire. This is the drift time. It can be measured by knowing the actual time of the particle passing. This can be achieved by installing an external trigger. The time difference between the trigger signal and the measurement of the signal in the drift tube can therefore be determined and used as the drift time. Therefore also the drift radius can indirectly be determined.

4.2 Trigger

Drift tubes require an external trigger to determine the drift time of a particle. Scintillators and photomultipliers (PMTs) are usually used for this purpose. When a particle travels through a scintillator, it excites the material which as a result emits photons. The scintillator is covered in reflecting foil so the light is trapped and led to the PMT. Upon collision with the photocathode, a primary electron is emitted. Inside the PMT, the electron is then accelerated by an electric field to the photodynodes, electrodes that amplify the electric signal by emitting additional electrons. The tube is evacuated to prevent the electrons from interacting with gas atoms. A PMT has several dynodes arranged so that after each collision the incoming electrons and the newly emitted electrons are directly attracted to the next dynode. After this amplifying effect, the electron avalanche reaches the anode where the signal can be recorded. The whole process is visualized in figure 4.2. Usually two scintillator plates are used in coincidence. One is positioned in front of the drift tube and one behind, relative to the expected track of the particle. This increases the probability of the by the trigger detected particles actually passing the drift tube. Another purpose is to filter out noise of the PMTs.

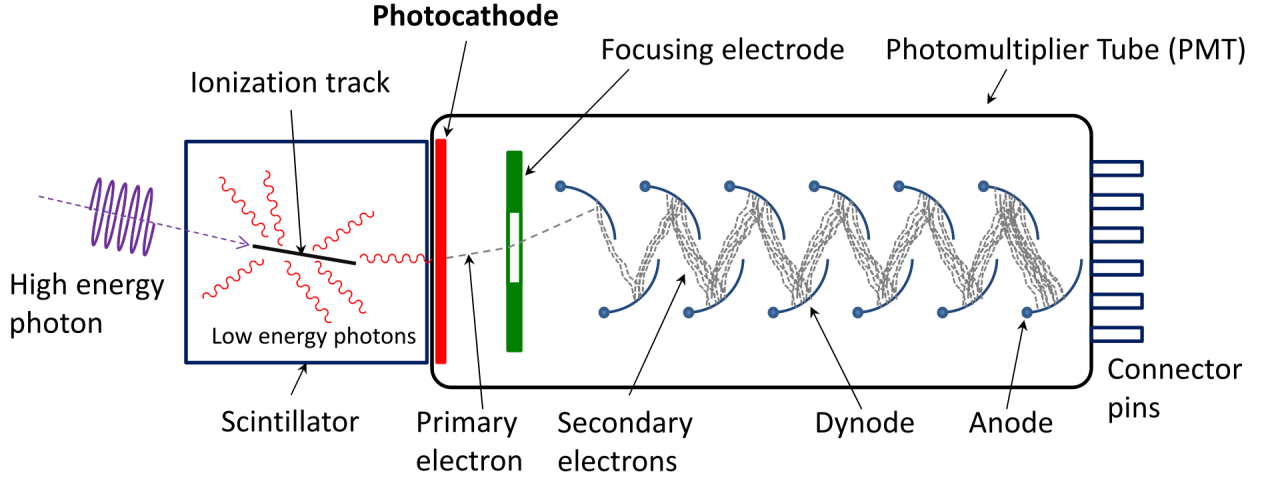


Figure 4.2: The working principle of a PMT in combination with a scintillator [16].

4.3 Gas Ionization

When a charged particle passes through a drift tube, it will interact with the drift gas, most importantly by ionizing it. There are two ionization mechanisms, the primary and the secondary ionization. The primary ionizations are a direct result of the particle interacting with the gas, therefore only occur along the track of the particle. An example for that is given in equation (4.1) where a muon μ^- encounters an atom A and transfers an energy higher than the binding energy to release an electron from the atom's shell. With sufficient kinetic energy these electrons can cause secondary ionizations, shown in equation (4.2) [17].



The primary interactions will result in an energy transfer from the particle to the gas. The mean energy loss of the particle per distance can be described by the Bethe formula:

$$-\left\langle \frac{dE}{dx} \right\rangle = \frac{4\pi r_e^2 m_e c^2 N_A Z \rho z^2}{A \beta^2} \left(\ln \left(\frac{2 m_e c^2 \beta^2}{I \cdot (1 - \beta^2)} \right) - \beta^2 - \frac{\delta}{2} \right) \quad (4.3)$$

Using the following parameters:

$r_e =$ electron radius	}	Physical constants
$m_e =$ electron mass		
$N_A =$ Avogadro number		
$Z =$ atomic number	}	Target parameters
$\rho =$ density		
$A =$ mass number		
$I =$ mean excitation energy		
$\delta =$ density effect	}	Particle parameters
$z =$ charge		
$\beta =$ relative velocity, $\beta = \frac{v}{c}$		

However, the Bethe formula is only applicable if the particle is heavier than an electron since the equation (4.3) mainly describes the interaction of heavy particles with shell electrons. To a large extent, electrons lose their energy via bremsstrahlung. The energy loss via the Bethe formula is an average, with the fluctuation being Landau distributed. The minimum of the formula is around $\beta\gamma \approx 3$. Particles with that energy are called Minimal Ionizing Particles (MIPs). Particles with this specific energy lose only a minimal amount of energy. The atmospheric muons used for this experiment can be approximated as MIPs for a broad energy range.

If a photon interacts with the gas, the interaction depends on the photon's energy, the ranges for the different effects are visualized in figure (4.3). In comparison to a heavy particle which produces many ionization events, a photon most commonly produces only one. In lower energy ranges the photoelectric effect dominates, where the photon is absorbed by a shell electron and all its energy is used to ionize the atom. For higher energies Compton scattering, where the photon only transmits part of its energy to the electron, and pair production occur.

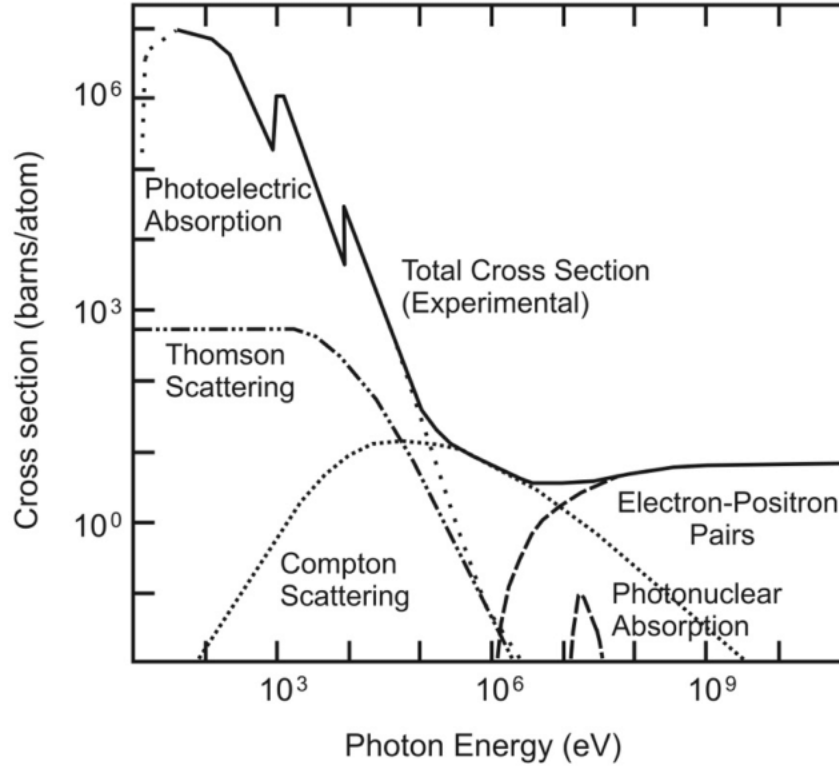


Figure 4.3: Energy dependent cross sections for photon interactions [18].

4.4 Electric Field

The electric field E is responsible for the drift but also for the amplification of the signal. In theory it is radially symmetrical around the wire. To calculate such an electric field one has to assume two coaxial cylinders, the tube as the outer one with a radius of r_t and the wire with a radius of r_w . The wire is on a positive potential U , while the tube is on ground potential. The integrated form of Gauss's law can be used, given in equation (4.4). Here, ε denotes the permittivity of the dielectric and ε_0 denotes the electric constant.

$$\oint_{\partial V} \vec{E} \cdot d\vec{A} = \frac{q}{\varepsilon\varepsilon_0} \quad (4.4)$$

With the assumption that the length of the tube $L \gg r_t$ and with the radial symmetry implying $\vec{E} \parallel d\vec{A}$, one can conclude

$$\oint_{\partial V} \vec{E} \cdot d\vec{A} = \int_0^L \int_0^{2\pi} E(r) r d\psi dz = 2\pi r \cdot L \cdot E(r) = \frac{q}{\varepsilon\varepsilon_0} \quad (4.5)$$

$$\Rightarrow E(r) = \frac{q}{2\pi r \varepsilon \varepsilon_0 L}. \quad (4.6)$$

Additionally, the electric potential is given by

$$U = \int_{r_w}^{r_t} E(r) dr \stackrel{(4.6)}{=} \int_{r_w}^{r_t} \frac{q}{2\pi r \varepsilon \varepsilon_0 L} dr = \frac{q}{2\pi \varepsilon \varepsilon_0 L} \cdot \ln\left(\frac{r_t}{r_w}\right). \quad (4.7)$$

Combining the expressions (4.6) and (4.7) results in the electric field being described by

$$E(r) = \frac{U}{r \cdot \ln\left(\frac{r_t}{r_w}\right)}. \quad (4.8)$$

The electric field increases thereby linearly to the applied voltage U and antiproportionally to the wire distance r .

4.5 Drift Gas

The drift gas serves multiple purposes and therefore is usually a mixture of different components. Since it has to be ionized easily, noble gases are suitable. Noble gases provide a high density of primary ionizations since they have a maximum of minimally bound electrons in their outer shells. Another advantage of using a noble gas is its low reactivity so that the gas does not corrode wire and tube wall. Additionally, a quenching gas is needed to absorb emitted photons. The photons are in an UV range and the result of transitions in the noble gas. It is necessary to absorb these photons because they have a high enough energy to free more electrons which would distort the signal. The quenching gas absorbs these photons via nonradiative transitions.

In order to maximize the number of ionizations per event the gas needs to have a high nuclear charge Z . Heavier gases have a higher number of electrons per volume in general. Maximizing the number of ionizations is especially important because the drift tube should be able to detect muons which are Minimal Ionizing Particles (see section 4.3). Other requirements of the gas are the stability and being relatively cost-effective. Suitable options are argon, xenon and krypton with argon being the cheapest. The ideal quenching gas depends on the noble gas. The quenching gas needs to absorb specific argon transitions since the thereby emitted photons have enough energy to ionize the cathode atoms. For

argon a suitable quenching gas is carbon dioxide [19].

4.6 Gas Gain

As already discussed in sections 4.5 and 4.4, the amplification of the signal in the gas is dependent on the properties of the drift gas, especially its mean free path, but also on the electric field. The acceleration of the electrons is directly proportional to the electric field. A high field strength therefore leads to electrons reaching the ionizing energy of the gas faster. The pressure of the drift gas at room temperature causes a mean free path of a few μm . The charge is multiplied according to the Townsend coefficient α_T [20] with which the relative gain dN/N is given by

$$\frac{dN}{N} = \alpha_T \left(\frac{E}{\rho}, \rho \right) dr. \quad (4.9)$$

The Townsend coefficient depends on the reduced electric field strength $\frac{E}{\rho}$ and the density ρ . One has to measure the Townsend coefficient as it cannot be calculated. The absolute gas gain G (4.10) is defined by the integral over equation (4.9).

$$G = \frac{N_f}{N_0} = \exp \left(\int_{r_{min}}^{r_w} \alpha_T(r) dr \right) = \exp \left(\int_{E(r_{min})}^{E(r_w)} \frac{\alpha_T(E)}{dE/dr} dE \right) \quad (4.10)$$

In (4.10), N_f/N_0 denotes the ratio of free electrons after the charge multiplication to the number of electrons before. r_{min} is the starting point of the amplification.

Expressing the electric field E in (4.10) with (4.8), the gas gain is defined as

$$G = \exp \left(\frac{V}{\ln(r_t/r_w)} \int_{E(r_{min})}^{E(r_w)} \frac{\alpha_T(E)}{E^2} dE \right). \quad (4.11)$$

It follows that the gain is dependent on the wire diameter with a higher gain for thicker wires. The starting point r_{min} is in a range between wire diameter and tube diameter.

4.7 Signal Characteristics

The signals transmitted in the drift tube are electromagnetic waves. The signals are a result of electrons from ionization events reaching the wire. These electrons then travel as

electric current along the wire towards the readout electronics. Their original signal form can be altered by effects like attenuation, delay and reflection. Electromagnetic waves are influenced by the wave impedance. This is defined as the ratio of transverse components of electric and magnetic fields in a plane wave. Usually the wave describes free waves, for signals travelling through a cable the characteristic impedance is of importance. The impedance is defined by

$$Z = \sqrt{\frac{R + i\omega L}{G + i\omega C}}. \quad (4.12)$$

In equation (4.12) R denotes the resistance, ω the angular frequency, L the inductance, G the conductance and C the capacitance. Since the tube is operated with direct current, $\omega = 0$, Z is solely dependent on R and G , allowing eq. (4.12) to be simplified to

$$Z = \sqrt{\frac{R}{G}}. \quad (4.13)$$

The specific tube geometry can be approximated as an coaxial cable for which the characteristic impedance is given as

$$Z = \frac{Z_0}{2\pi\sqrt{\varepsilon_r}} \ln\left(\frac{r_t}{r_w}\right), \quad (4.14)$$

with the vacuum wave impedance $Z_0 = \sqrt{\mu_0/\varepsilon_0}$ and the relative permittivity $\varepsilon_r \approx 1$ for the used composition of argon and carbon dioxide. A high characteristic impedance results in an attenuation of the signal. For the used drift tubes the characteristic impedance can be calculated for both wire diameters that were used.

$$Z = \begin{cases} 365.6 \Omega, & \text{for } r_w = 45 \mu\text{m} \\ 389.9 \Omega, & \text{for } r_w = 30 \mu\text{m} \end{cases}$$

Since the impedance acts at all positions of the wire, the attenuation is dependent on the length the signal has to travel through.

Another signal altering effect is the reflection which is the result of a changing wave impedance. At the end of a drift tube the signal is reflected if the characteristic impedance of the wire is not matched to the terminating resistance. If the wire is not terminated, reflection at an open end occurs, where the entire signal is reflected. Depending on the signal length and the speed of the signal this might result in interference [21].

Chapter 5

Experimental Setup

The test station (see figure 5.1) was built to test the straw tubes that are planned to be used for the muon spectrometer at SHiP. It serves as an opportunity to characterize their properties and optimize the reconstruction of the muon tracks. For that two drift tube modules as well as two $110\text{ cm} \times 55\text{ cm} \times 2.5\text{ cm}$ scintillator plates on top and under the straw tubes were used as a reference. The modules are designed based on the modules of the OPERA experiment [22]. For simplicity, they will be called OPERA modules in the following. The OPERA modules consist of each 48 drift tubes. The aluminium drift tubes are arranged in a 4×12 block, have an outer diameter of 28 mm and a wall thickness of $850\text{ }\mu\text{m}$ [23]. The size of the scintillator plates is specifically selected so that they cover the OPERA modules.

5.1 Straw Tubes

The test station includes five straw tubes made out of mylar and coated with 20 nm Cu and 50 nm Au. These are divided in a Single Straw Prototype and a Quad Straw Prototype. The straws have a diameter of 20 mm and a length of 5 m. For the Quad Straw Prototype, straw 1 and 3 in figure 5.2 have a wire with a diameter of $30\text{ }\mu\text{m}$ while the wires of straw 2 and 4 have a diameter of $45\text{ }\mu\text{m}$. This is because the wire thickness for the actual experiment has not yet been decided [24]. All wires are made out of gold coated tungsten. The straws are mounted between two aluminium plates and stretched by 2 cm. This was done to reduce sagging of the straws. Also the wires inside the straws are stretched. The straws are connected to a L3 amplifier operated with 4 V. This is due to the signals created by a passing particles is in a range of only a few μV . The amplifier has 4 amplifying channels,



Figure 5.1: The test station including straw tubes, OPERA modules, drift gas tank and amplifier. The readout electronics are located on the left. The straws have a length of 5 m.

one for each straw tube. For each channel the amplifier has two outputs. One output is the amplified signal in its original form, for the second output the signal is inverted thus positive. The amplification can result in cross talk between the 4 different channels where the signal of one channel leads to a peak in another without the an actual event in the related straw. The straws are operated with a high voltage around 2000 V. An accurate setting of the HV is essential for the analysis of the data, because the average signal size needs to be the same for all wires. From equation (4.11) it follows that the wire radius has an effect on the gas gain and therefore also on the signal size. The applied HV was therefore different depending on the diameter of the wire. For optimum operation, a HV of around 1950 V is set for the 30 μm wire and 2175 V for the 45 μm wire [25].

5.2 Signal Sources

For this set up two different sources were used. The first is a Fe-55 source emitting gamma rays with an average energy of 5.89 keV [26] and an activity in an order of 100 kBq. This activity is high enough to keep the measurement time to only a few minutes. However, it is still low enough to not create several pulses in the 1024 ns long measurement window.

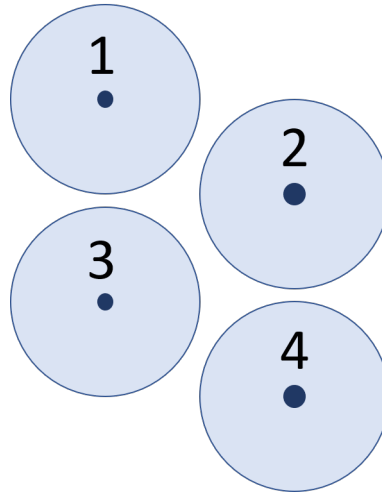


Figure 5.2: A cross section of the arrangement of the straws. Straw 1 and 3 have a smaller wire diameter of $30\ \mu\text{m}$, while straw 2 and 4 have a wire diameter of $45\ \mu\text{m}$.

Atmospheric muons are used as the second source. These muons are produced in the upper atmosphere when cosmic particles interact with air molecules. The cosmic particles mainly consist of protons and helium nuclei. The interactions result in particle showers with common secondary particles being neutrons, protons and pions. Pions mainly decay into muons which despite their short lifetime of approximately $2.2\ \mu\text{s}$ can reach the ground due to their highly relativistic speed. At ground level the muons have an angular distribution of $\cos(\theta)^2$.

5.3 Trigger Setup

To compare the muon signals at different position of the straws, a movable external trigger, visualised in figure 5.3 is used. It consists of two $3.7\ \text{cm}$ wide and $30\ \text{cm}$ long scintillator plates and it can be mounted at a variable position onto the test station. Those plates have a distance of $10\ \text{cm}$ to each other and are both equipped with PMTs. Both signals from upper and lower scintillator plate are in coincidence meaning only if both plates detect a signal simultaneously an event is counted.

Approximately there are 100 muons per square meter and second. The external trigger has an area of $3.7\ \text{cm} \times 30\ \text{cm} = 111\ \text{cm}^2$ and the muons are only triggered if they are passing through both scintillator plates so the tracks must be sufficiently vertical and

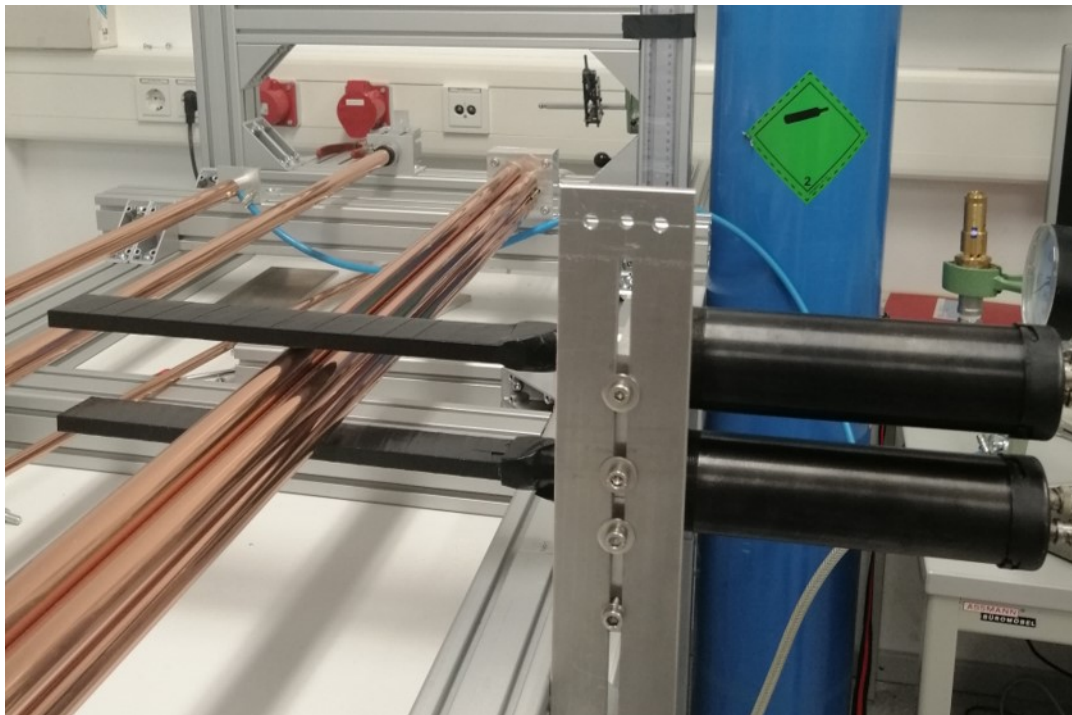


Figure 5.3: The external trigger used to detect muons in a horizontal set up.

because of their angular distribution, most muons are not counted. This results in a trigger rate of around 1 Hz. Also because the straws are relatively small in diameter, most triggered muon events were not detected by the straws. This small cross section of tube and trigger is the disadvantage of the vertical trigger set up. With a parallel set up one could drastically increase the cross section but since the measuring distance was 50 cm and the trigger would detect muons along the distance of 30 cm, the segmentation per length would not be as accurate.

5.4 Gas System

For the prototype the gas mixture used is 80% argon and 20% CO_2 . The gas tank is connected to an adjustable pressure reducer. The Straws are intended to operate under normal, atmospheric pressure of approximately 1 bar. The flow is regulated by the flowmeter with the intensity of the gas flow indicated by the bubbler. It diverts the gas into an oil, producing bubbles and therefore making the intensity of the flow visible. The bubbler also regulates the pressure inside the straws. The gas is directed successively through all straw tubes and OPERA modules.

5.5 Electronics

The data of the straw tubes was recorded by a CAEN V1720 Flash Analog to Digital Converter (FADC). It transforms the voltages of the signal into data that can be stored on the connected computer. The FADC uses a ring buffer that stores the last 1024 samples. It records continuously with a sampling rate of 250 MS/s. Each sample has a resolution of 4 ns. Only if the trigger indicates an event, the signal is permanently stored. The FADC has a 12 bit resolution. The reference voltage is currently set from -1 V to 1 V. For storing the FADC uses a conversion factor C of

$$C = \frac{4096}{2V}, \quad (5.1)$$

which results in an arbitrary unit, in the following used as a.u., for the signal amplitude. Since only the incidence of a trigger signal but not its shape is of relevance, the signals are discriminated and adapted to the NIM standard [27]. This results in an identical binary signal for each PMT signal. The signals are connected via a logical AND gate that checks if both PMTs coincidentally transmit a signal. Only then an event is counted and the FADC stores the last 1024 samples. Note that in the following instead of sample, the term bin is used. After the AND gate, the PMT signal is connected to a gate generator serving as a trigger busy. Therefore, the signal is elongated so that a second event directly after the first is not counted. This is because while the PMTs can record multiple events at once, the FADC can not separate these. The program CAEN WaveDump is used to read out the FADC data.

Chapter 6

Measurements and Analysis

The goal of this thesis is to characterize the signal evolution by comparing events at different positions along the straw's length. This can be used to quantify the effects of attenuation and reflection. This series of measurements was once performed for muons and once performed for gamma rays. This was because both methods have their specific advantages and disadvantages that are further discussed on the next pages. For the measurements the Quad Straw Prototype was used. This prototype is usually used to test tracking properties but since the event rate is so low with this trigger set up, the additional data from more straw tubes decreases the measurement time needed to gain more statistics. Although all straws are relatively similar, a comparison is only partially possible due to their different wires. The data of the straws were recorded in one channel each. Straw 1 was assigned to channel 0, straw 2 to channel 1, et cetera. A defective output caused that for channel 3 the actual signal could not be read out, so that the output for the inverted signal had to be used.

6.1 Signal Characterization using Atmospheric Muons

The straws of the SHiP Spectrometer Straw Tracker will be used determine the momenta of charged particles. Therefore it is also relevant for the prototype to use similar particles as an ionization source. For this purpose, atmospheric muons are used. They do not require a direct source and similar signals are expected in the actual experiment. Only a limited amount of atmospheric muons reach the earth per area and time therefore the time to measure one position was several days.

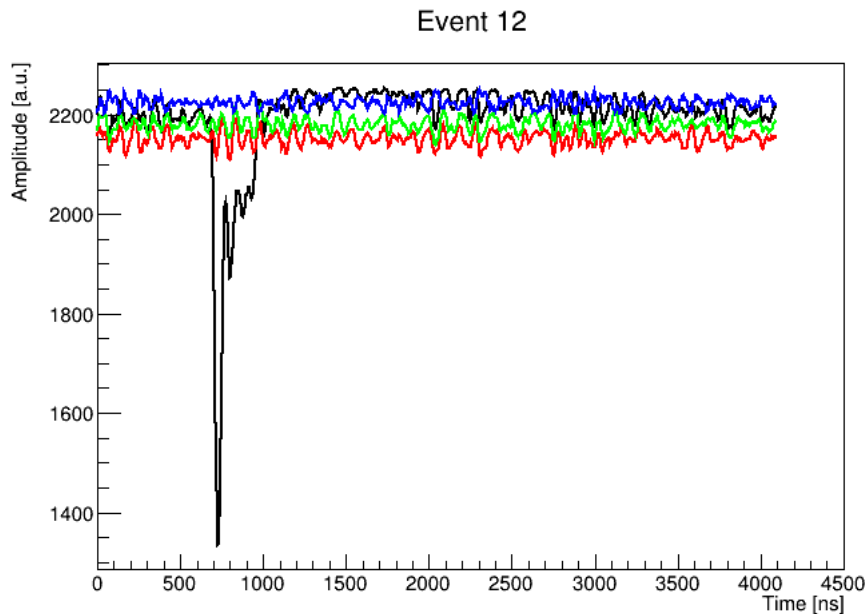


Figure 6.1: Example of a typical muon signal. The four straws are shown here in the four different colors. Only a hit in channel 0 (black) was detected. A high first peak and several smaller afterpulses are visible.

6.1.1 Muon Signals

In figure 6.1 a single muon event is visualized. Generally one has to note that muon signals vary in shape and height a lot more than gamma signals from the used Fe-55 source. This is because the number of primary ionizations is not set but Landau distributed (see section 4.3). The settings for the HV with which the tubes were operated have to be precisely adjusted as this can lead to saturation effects of the L3, an example is given in figure 6.2. Note that the saturated signal is inverted because it is from channel 3. There were two series of measurements taken for the muons, one with the HV set to 1995 V for tube 1 and 3 and to 2195 V for tube 2 and 4, and one with a HV of 1800 V for tube 1 and 3, and 2000 V for 2 and 4. The variation of the HV between the four straws was used because the wires of the straws do not have the same diameter. To achieve equal signal heights between the straws the HV has to be adjusted. The range of the used signal minima is from 1900 to approximately 600 arbitrary FADC units (a.u.), converted using equation (5.1). Other important properties to characterize the signal shape are the width of the signal and the drift time. The width in this case is not measured as a physical length but as a period of time. Going back to figure 6.2 one can notice that after the signal a tail is recorded where the signal drops below the actual baseline for a period of time. This shifted baseline is

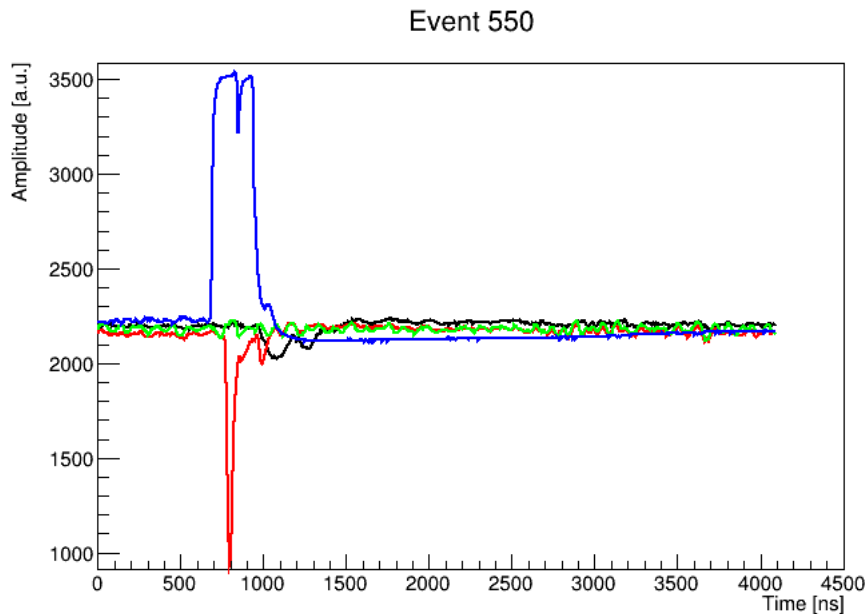


Figure 6.2: Example of a saturated muon pulse in channel 3 (blue). Note that the channel is inverted due to defective readout electronics. One can clearly see that the normally thin peak is severely widened. Another event can be seen in channel 1 (red).

the result of charge conservation [28]. Usually one event has several peaks with the first usually being the biggest. This is because the number of ionization clusters reaching the wire is larger for shorter drift times.

6.1.2 Drift Time

For muon tracking the drift time (see section 4.1) is the most important parameter. To further illustrate the concept of the drift time one can once again look at figure 6.1. There the drift time is approximately 700 ns. Since the drift time varies, one can visualize a drift time spectrum as in figure 6.3. In the following the time is not given in ns but in bins, with one bin being one sample of the FADC (see section 5.5 for the unit conversions of the FADC). For reference the drift time is typically in a range from 160 to 500 bins with high drift times occurring less. The drift times are relative to the readout time of the FADC ring buffer so that the smallest realistic drift times are around 160 ns.

The signal height is dependent on the drift time. For example, a small drift time implies more primary ionizations, which means the signal is larger. This follows from the fact

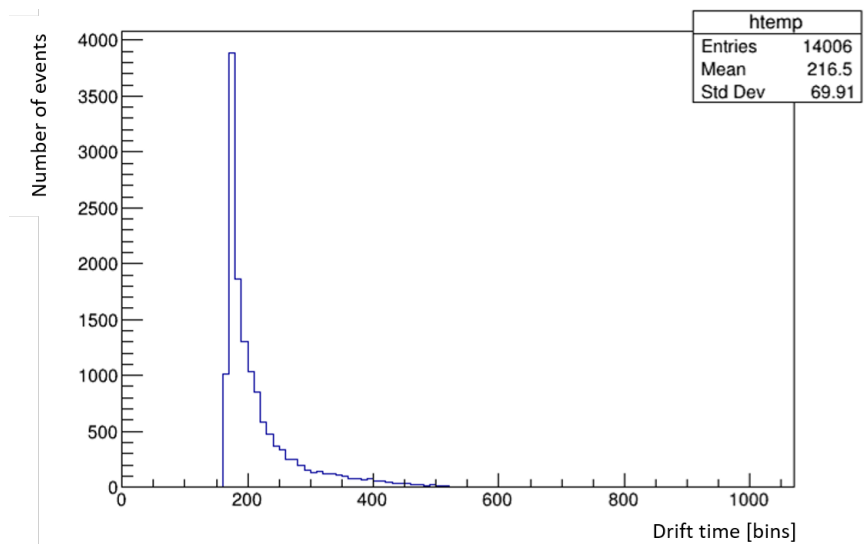


Figure 6.3: A drift time spectrum for muon events. For 14 000 events, the drift times were determined in bins and plotted according to the number of times they occurred. The most frequent drift times are around 200 bins, lower values than 160 bins do not occur, but larger drift times up to 500 bins do.

that a muon travels a longer distance through the tube when it passes close to the wire.

6.1.3 Muon Signal Evolution

One has several options to quantify the signal evolution along the straw. The recorded signal corresponds to the total charge. Due to charge conservation, the integral over the entire period is therefore 0. Forming a definite integral over the bin entries is therefore only of limited significance. Instead, it is possible to look at the indefinite integral or simply to quantify the signal evolution with the help of the peak height. The second approach was implemented. The initial HV was determined for signals going through the straw close to the read out electronics. With the assumption that the signals will decrease in height for an increased travelling distance, the HV was set to amplify peaks close to the saturation level. The trigger was positioned at nine locations along the straws, starting for the first data set at 0 cm and for the second at 50 cm, moving in 50 cm steps to 500 cm. For the first data set, the position of 400 cm was removed because at the time of the measurement the tubes were not completely filled with gas. For each of these positions the data was acquired over a minimum of two days.

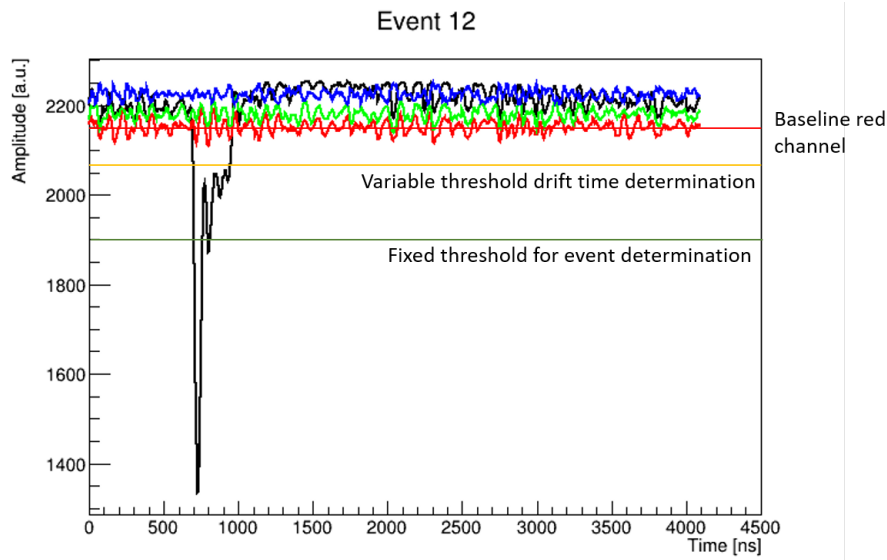


Figure 6.4: The same example event of a muon pulse as figure 6.1 but with drawn in thresholds and an example baseline for the red channel.

Moun Signal Analysis Script

For the analysis a first converting script was used converting WaveDump's binary data format into a root file [29], merging the data of all four straws into one file and calculate basic characteristics for each event such as minimum and drift time. This was to gain a quick overview over the data and evaluate the quality. From there a second script determined the characteristics more accurately.

At first the baseline was calculated individually for each event using the first 100 entries, an example for such a baseline is visualized in figure 6.4. With the baseline the signals were then not only inverted but also shifted to a new baseline of zero. A low initial peak means that the now calculated maximum is high.

Next the drift time was calculated by finding the start of the signal. For that one has the option to set a fixed threshold or one can calculate a percentage of the maximum. Since the signal is not abruptly at its maximum but rises for some time depending on the peak height, simply using the maximum as the point to calculate the drift time would distort the drift time. As a consequence one has to choose a low enough threshold to find the exact beginning of the signal but it needs to be high enough to not use the noise. Many events did not contain a muon signal due to the muon flying through the trigger but not

the straws. Also a lot of events were empty due to the muon flying through one straw the data resulting in the recording of all four channels. Therefore, the determination of the drift time via a percentage of the maximum is only possible the empty events are filtered out before. Otherwise that would have resulted in short, nonzero drift times for the empty events. Another disadvantage is the imprecise determination of the rising point, because for large signals the point is later than for small signals. A different option to calculate the drift time is to determine the beginning of the signal by the exceeding of the noise. This requires the standard deviation of the baseline, which, since there were still some noise peaks above it, was multiplied by a factor of four. This variable threshold for the drift time determination is visualized in 6.4. This option has been implemented because it leads to more accurate signal starting points. Additionally to filtering out events with an unrealistic drift time (e.g events with an calculated drift time under 160 bins), only events were used with an maximum peak over a threshold of 200 a.u.. This is to ensure that only actual muon events were used for the analysis and no noise that was randomly above the threshold for the drift time calculation. Although this would be very unlikely, noise has been observed in a range up to about 100 a.u., which could theoretically exceed the threshold and be included in the drift time calculation.

Since the saturation of the signals was a big problem, only a part of the signals was considered for the formation of an average value. Since the ionization follows the landau distribution, the pulse height also follows the landau distribution. The mean value and the standard deviation of a landau distribution are undefined. Simply calculating a mean results a deviation from the true mean. Therefore it makes sense to form a truncated mean [30]. For this truncated mean 10 % of the smallest and 30 % of the largest peaks are excluded from the averaging process. This truncated mean reduces the deviation from the true mean the most. Since it is applied to all results, the peaks that go into saturation are reduced equally for all distances.

For each channel, the events were then divided into three drift time ranges of equal size. The intervals chosen were (160 - 200), (200 - 240) and (240 - 280), with all values given in bins. This subdivision leads to more accurate average values for the peak height since different long drift times lead to different high pulses.

Results of the Signal Evolution

The plots visualized in figures 6.5 and 6.6 show the average peak height for the different positions. The data was divided according to HV setting, channel and drift time range. figure 6.5 shows two data series with a high voltage of 2195 V/ 2195 V. Here and in the following the HV will be given in this notation for the two different wire diameters. It becomes clear that a few positions, here especially the position at 300 cm, deviate from the overall trend. For the measurement series with a lower high voltage of 1800 V/ 2000 V, shown in figure 6.6, there are no large deviation, but there is also no clear trend of the signal evolution. Not all signal evolutions are shown here. A selection of other drift time ranges and channels the figures can be found in the appendix A.

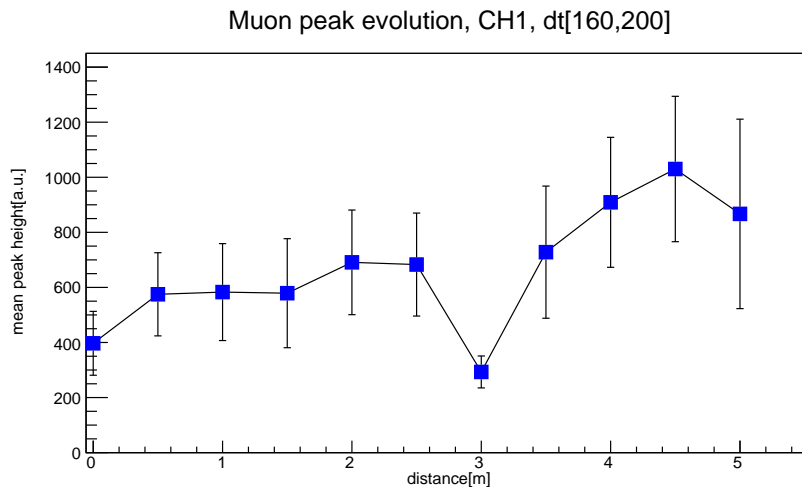


Figure 6.5: Signal height evolution for muon events. Here visualized is channel 1 in a drift time range of (160 - 200), with the HV set to 1995 V/ 2195 V.

Discussion

The fact that no clear trend can be seen for the muons is probably due to several factors. It is obvious that a clear weakening effect in the form of an exponential drop, as one would expect according to the cable impedance, can not be observed. Although for some data series a slight attenuation can be observed, for more data series an increase can be seen. However, this is not to as significant extent as the variation in signal height is in the same order of magnitude as the errors of the individual data points. That the errors are so large has several reasons. On the one hand the signal shape varies strongly between the individual muon events and on the other hand no Gaussian distribution is given, which

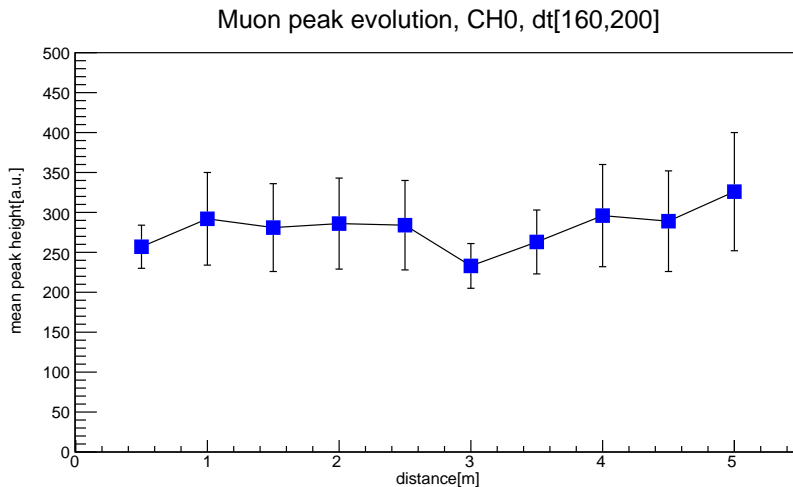


Figure 6.6: Signal height evolution for muon events. Here visualized is channel 0 in a drift time range of (160 - 200), with the HV set to 1800 V/ 2000 V

has the consequence that a standard deviation can not be used as an error without further justification. By forming a truncated mean, the Landau distribution is trimmed and can be approximated with a Gaussian distribution. Therefore the standard deviation was nevertheless used as a measure of the error.

Reasons for the fluctuations between the different positions can be changed conditions due to the long measurement time. An example is an insufficient gas supply due to an empty gas bottle. However, the greatest inaccuracy will be in the small measurement window. Only signals above a certain threshold are included and there is a maximum size for signals. It is important that the maximum of the signal height distribution lies in the measurement window. In the measurement series with the higher HV, however, there were some positions given where a large part of the events was saturated. These were truncated in order to reduce the fluctuation but at the expense of higher statistics. The individual data sets sometimes have only around 1000 events, which limits the statistical significance of these.

6.2 Signal Characterization using Gamma Rays

Since the data acquisition for the muons takes a very long time and the signal shapes largely fluctuate, also a gamma source was used. As with the muons, two measurement

series were taken. The source was placed at a distance of about 10 cm from the tubes and moved in 25 cm steps along the tubes. A total of 19 positions were examined for the first measurement series, starting at 25 cm, leaving out the measurement at 275 cm since there was the scaffold of the OPERA modules and with the last position being at 500 cm. For the second measurement series all 20 positions were examined. Since the source has a high activity the overall measurement time was significantly shorter compared to the muon measurements. In less than 5 minutes 100 000 events are recorded. A self-trigger was used, which triggered on signals from the straws that were larger than a set threshold of 1900 a.u., thus a deviation from the baseline of 300 a.u.. Therefore, in contrast to the muon events, for each event there is a peak in one of the channels.

In the first measurement series, the HV was set very low and the threshold for triggering was too high. This narrow measurement window caused the mean pulse heights to converge, especially for small distances, because there the mean values for the peak heights probably were below the threshold. The resulting systematic error was reduced in the second measurement series both by higher HV, which was then calibrated to the signals at short distances, and by a lower threshold.

6.2.1 Gamma Signals

Compared to muon signals, gamma signals have a very uniform pulse shape. Their height, the parameter of interest, depends not solely on the position along the straw but also on the distance of the ionization event inside the straw. This is because the photons transmit their entire energy in a single ionization event. This is also the reason no trigger was used as the detection of the photon by the trigger would be the only ionization event. Therefore no drift time can be calculated. Still the signal height depends on the location of the ionization event inside the tube, so that for the same position along the straw the signal height still varies. In figure 6.7 an example of a typical gamma pulse is given.

6.2.2 Gamma Signal Evolution

The processing of the collected measurement data is similar to that of the muon signals. The signals were shifted by the baseline and inverted. For the resulting maximum, a threshold of 200 was chosen. Since the height of the pulses was not a Landau distribution but a Gaussian distribution, a mean and standard deviation can be determined. It is

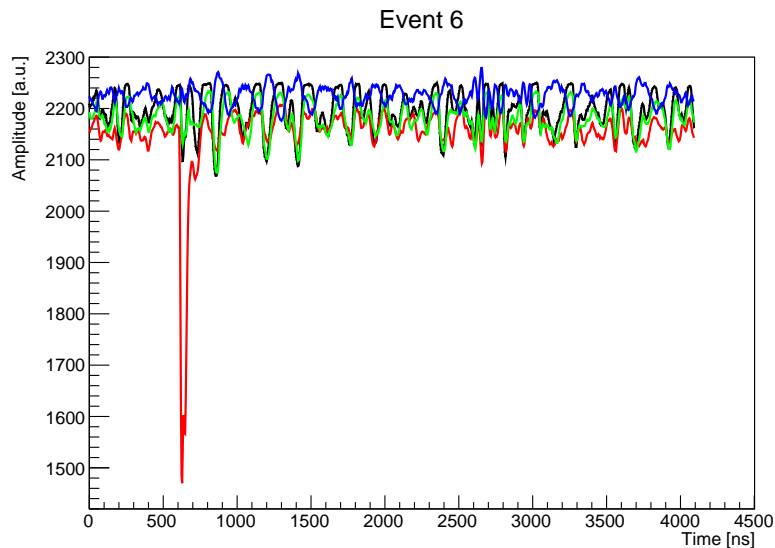


Figure 6.7: Example of a gamma signal in channel 1 (red). The channels are again shown here in the four different colors. The baseline of 2200 is visible.

not Landau distributed because for photons the Bethe formula (4.3) does not apply. In the plots in figure 6.8 and figure 6.9 the average peak height for the individual measured positions is displayed. Additionally, the standard deviation is plotted. A clear and steady

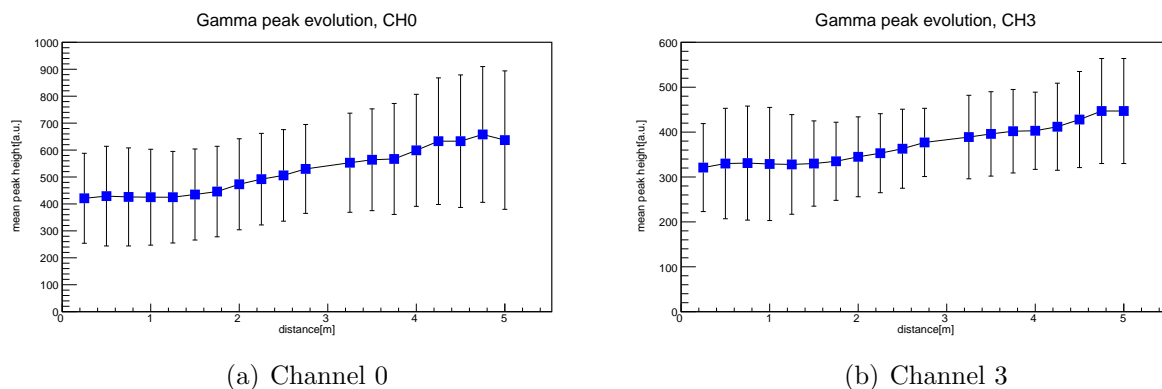


Figure 6.8: Signal height evolution for gamma events. Here visualized for channel 0 and 3, with the HV set to 1800 V/ 2000.

increase of the signal height with larger distance to the readout electronics can be seen for both HV settings. Furthermore in figure 6.10 and figure 6.11 the average of the the whole signal and not only the signal maximum was calculated for the different positions. This has been possible due to the uniform pulse shape of gamma signals. It should be noted

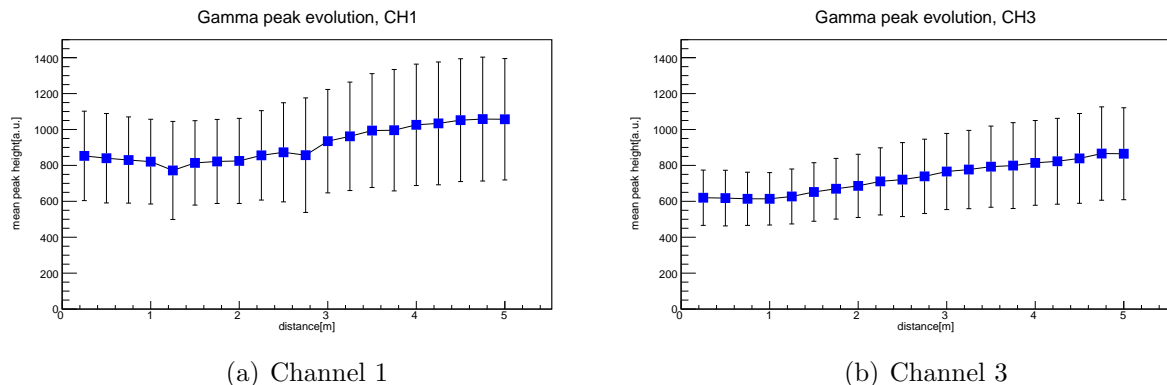


Figure 6.9: Signal height evolution for gamma events. Here visualized for channel 1 and 3, with the HV set to 1900 V/ 2100 V.

that the errors are not included in order to increase readability. It can be seen that for positions far away from the readout electronics, depicted here in green and blue, the signals are significantly larger than for smaller distances, depicted in orange and red. For channel 0, a small secondary pulse next to the maximum can be seen, which is more pronounced for larger distances.

6.2.3 Discussion

It was not expected that there would be an increase of the signal along the tube. The comparison of the signal height with its width suggest that the causing effect for this is probably the reflection. Most likely there was a superposition of the signals as the signal speed on the wire is in an order of magnitude with the speed of light. Therefore the signal can travel approximately 20 cm to 30 cm per nanosecond. This superposition is highest at positions far away from the readout electronics, where the signal and its reflection arrive almost simultaneously. At small distances, the reflection has a distance difference of several meters, so that the signals are no longer directly overlaid. figure 6.10 could indicate such a superposition. A slight narrowing of the signal width can be suspected. However this is not particularly significant due to the large errors. To quantify this narrowing effect also the signal width (FWHM) was measured. However the decrease in width for increasing signal peaks was not measurable.

There are similar sources of error for these measurement series compared to those of the muon measurement series. Here the measurement window was relatively small as well.

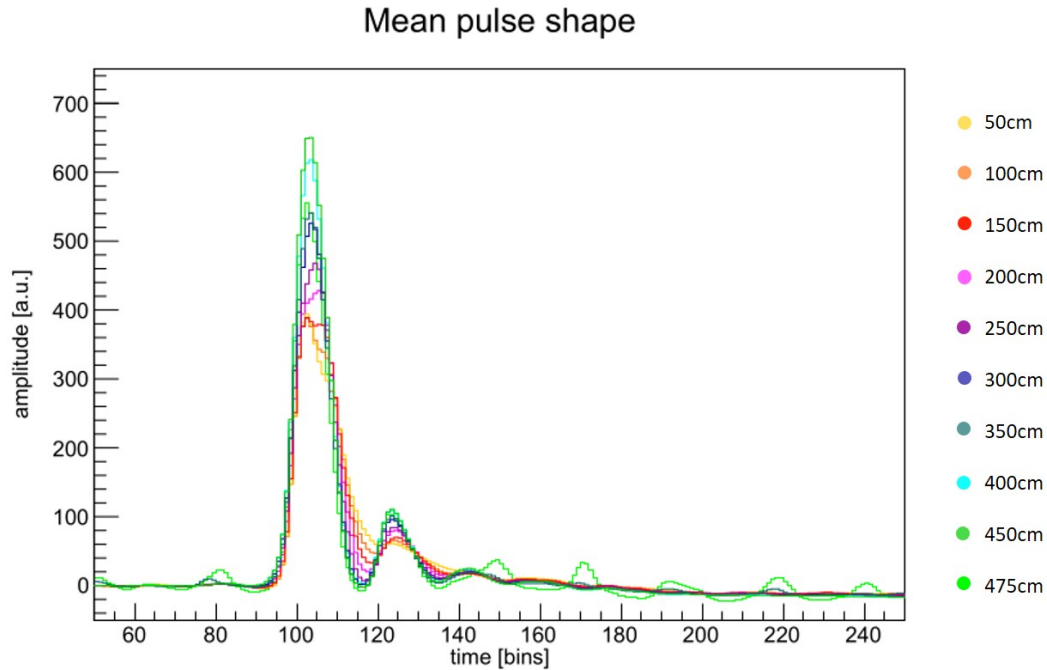


Figure 6.10: Average gamma pulse shape for Ch0. Here the signal is already inverted. One can notice an oscillation that increases for larger distances.

This is because of a low trigger threshold. Also the height of the HV has a significant influence on the accuracy of the mean values due to possible saturation.

In general the results for the gamma source are more accurate than the results for the muons because of the more uniform pulse shape. A signal amplification can be observed for gamma rays, depending on the distance the signal has to travel through the wire. Also, this effect will likewise be present for the muon signals, but not as prominent due to the large variance of the signals.

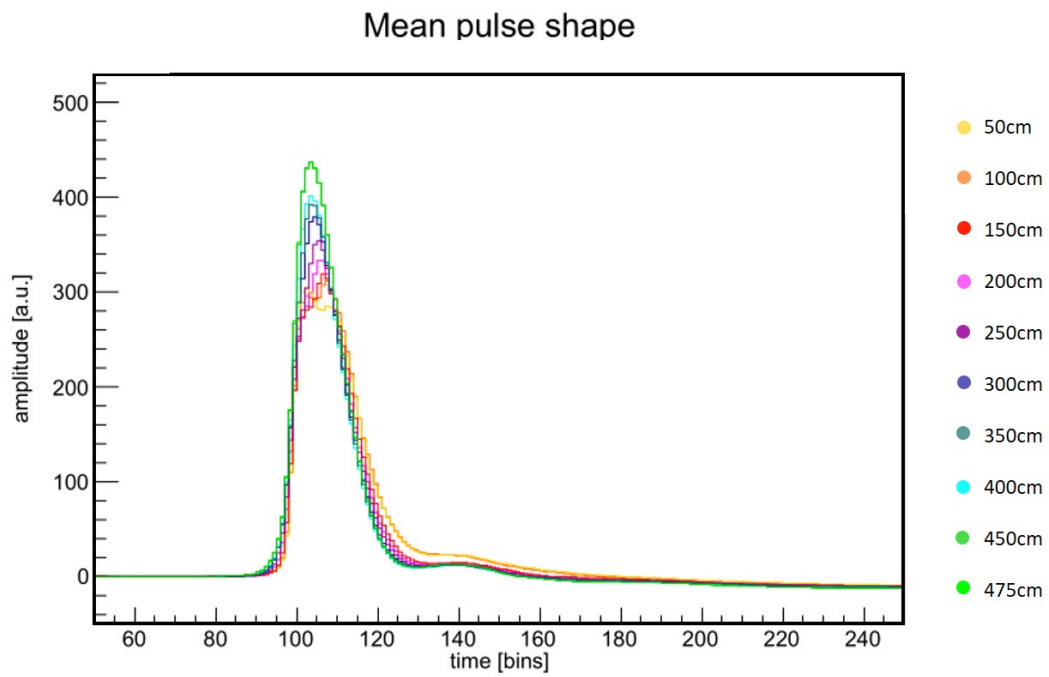


Figure 6.11: Average gamma pulse shape for Ch3. The signal is also already inverted.

Chapter 7

Summary and Outlook

For this bachelor thesis, signal evolution along the straws was recorded for different ionization sources and different operating voltages. Muon and gamma signals were recorded and analyzed. For the evaluation, the maxima were averaged, depending on the set HV, channel and for the muon signals also depending on the drift time. No significant signal change was observed for the muon signals. Whether this was due to the smaller amount of data, or whether there really is no trend, can only be clarified with further measurements, i.e. larger statistics. Sources of error will be the variable pulse shape and the saturation. A trend could be determined for the gamma signals. For the first measurement series with higher HV an amplification of 26.64 ± 2.76 a.u. per 50 cm could be determined. For the second series of measurements with a lower HV an amplification could only be observed for channels 1 and 3, this was at 23.29 ± 8.11 a.u. per 50 cm. For channel 0 and 2 no amplification could be observed. Since channel 0 and 2, as well as channel 1 and 3 are each connected together to a HV supply, the assumption of a systematic error is reasonable. Most likely, there is a superposition of the signal with its reflection. When the signal and its reflection reach the readout electronics almost simultaneously, the resulting signal is most intense. This happens when signal and reflection have to travel the same distance, i.e. at the end of the straw tube. As a result, higher signals are measured for positions located at the end of the straw tube.

It would be interesting to measure only the attenuation according to the characteristic impedance. For this, a terminating resistor would have to be installed, which has the same size as the characteristic impedance of the straw. In this way, a reflection can be prevented. It is of advantage to know the attenuation. The attenuation can e.g. have an influence on

the threshold for signal detection.

List of Figures

2.1	The Standard Model of particle physics [2].	8
2.2	Possible areas to search for new particles [8].	10
3.1	The SHiP detector [13].	13
4.1	Cross section of a drift tube.	15
4.2	The working principle of a PMT in combination with a scintillator [16]. . .	17
4.3	Energy dependent cross sections for photon interactions [18].	19
5.1	The test station	24
5.2	A cross section of the arrangement of the straws. Straw 1 and 3 have a smaller wire diameter of 30 μm , while straw 2 and 4 have a wire diameter of 45 μm	25
5.3	The external trigger used to detect muons in a horizontal set up.	26
6.1	Example of a typical muon signal	30
6.2	Example of a saturated muon pulse in channel 3 (blue).	31
6.3	A drift time spectrum for muon events.	32
6.4	Example muon event with drawn in thresholds.	33
6.5	Signal height evolution for muon events. Here visualized is channel 1 in a drift time range of (160 - 200), with the HV set to 1995 V/ 2195 V.	35
6.6	Signal height evolution for muon events. Here visualized is channel 0 in a drift time range of (160 - 200), with the HV set to 1800 V/ 2000 V	36
6.7	Example of a gamma signal in channel 1 (red). The channels are again shown here in the four different colors. The baseline of 2200 is visible. . . .	38
6.8	Signal height evolution for gamma events. Here visualized for channel 0 and 3, with the HV set to 1800 V/ 2000.	38

6.9	Signal height evolution for gamma events. Here visualized for channel 1 and 3, with the HV set to 1900 V/ 2100 V.	39
6.10	Average gamma pulse shape for Ch0. Here the signal is already inverted. One can notice an oscillation that increases for larger distances.	40
6.11	Average gamma pulse shape for Ch3. The signal is also already inverted.	41
A.1	Signal height evolution for muon events. Here visualized for channel 0 and 1, with the HV set to 1900 V/ 2100 V.	51
A.2	Signal height evolution for muon events. Here visualized for channel 1 and 2, with the HV set to 1900 V/ 2100 V.	52
A.3	Signal height evolution for muon events. Here visualized for channel 2, with the HV set to 1800 V/ 2000 V.	52
A.4	Signal height evolution for gamma events. Here visualized for channel 1, with the HV set to 1800 V/ 2000 V and for channel 2, with the HV set to 1900 V/ 2100 V.	52
A.5	Evolution of the pulse shape for gamma events. Here visualized for channel 1 and 2, with the HV set to 1900 V/ 2100 V.	53

Bibliography

- [1] Brian R Martin and Graham Shaw. *Particle physics*. John Wiley & Sons, 2017.
- [2] Wikipedia. *Standard model of elementary particles*. URL: https://en.wikipedia.org/wiki/Standard_Model#/media/File:Standard_Model_of_Elementary_Particles.svg (visited on 12/20/2020).
- [3] Raymond Davis, Don S. Harmer, and Kenneth C. Hoffman. “Search for Neutrinos from the Sun”. In: *Phys. Rev. Lett.* 20 (21 May 1968), pp. 1205–1209. DOI: 10.1103/PhysRevLett.20.1205. URL: <https://link.aps.org/doi/10.1103/PhysRevLett.20.1205>.
- [4] Y Fukuda et al. “Evidence for oscillation of atmospheric neutrinos”. In: *Physical Review Letters* 81.8 (1998), p. 1562.
- [5] G. Aad et al. “Observation of a new particle in the search for the Standard Model Higgs boson with the ATLAS detector at the LHC”. In: *Physics Letters B* 716.1 (2012), pp. 1–29. ISSN: 0370-2693. DOI: <https://doi.org/10.1016/j.physletb.2012.08.020>. URL: <http://www.sciencedirect.com/science/article/pii/S037026931200857X>.
- [6] S. Chatrchyan et al. “Observation of a new boson at a mass of 125 GeV with the CMS experiment at the LHC”. In: *Physics Letters B* 716.1 (2012), pp. 30–61. ISSN: 0370-2693. DOI: <https://doi.org/10.1016/j.physletb.2012.08.021>. URL: <http://www.sciencedirect.com/science/article/pii/S0370269312008581>.
- [7] J. H. Christenson et al. “Evidence for the 2π Decay of the K_2^0 Meson”. In: *Phys. Rev. Lett.* 13 (4 July 1964), pp. 138–140. DOI: 10.1103/PhysRevLett.13.138. URL: <https://link.aps.org/doi/10.1103/PhysRevLett.13.138>.

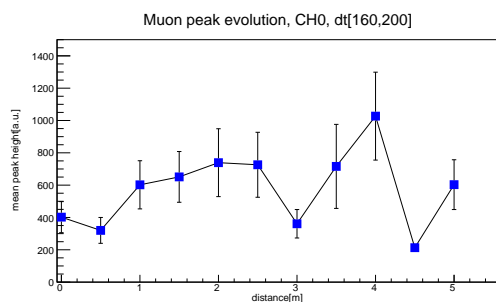
- [8] V. M. Gorkavenko. “Search for Hidden Particles in Intensity Frontier Experiment SHiP”. In: *Ukrainian Journal of Physics* 64.8 (Sept. 2019), p. 689. ISSN: 2071-0186. DOI: 10.15407/ujpe64.8.689. URL: <http://dx.doi.org/10.15407/ujpe64.8.689>.
- [9] Dmitry Gorbunov et al. “Heavy Neutral Leptons from kaon decays in the SHiP experiment”. In: *arXiv preprint arXiv:2004.07974* (2020).
- [10] Takehiko Asaka, Steve Blanchet, and Mikhail Shaposhnikov. “The MSM, dark matter and neutrino masses”. In: *Physics Letters B* 631.4 (Dec. 2005), pp. 151–156. ISSN: 0370-2693. DOI: 10.1016/j.physletb.2005.09.070. URL: <http://dx.doi.org/10.1016/j.physletb.2005.09.070>.
- [11] Laurent Canetti and Mikhail Shaposhnikov. “Baryon asymmetry of the Universe in the MSM”. In: *Journal of Cosmology and Astroparticle Physics* 2010.09 (Sept. 2010), pp. 001–001. ISSN: 1475-7516. DOI: 10.1088/1475-7516/2010/09/001. URL: <http://dx.doi.org/10.1088/1475-7516/2010/09/001>.
- [12] Samoil M Bilenky, J Hošek, and ST Petcov. “On the oscillations of neutrinos with Dirac and Majorana masses”. In: *Physics Letters B* 94.4 (1980), pp. 495–498.
- [13] C. Ahdida et al. *SHiP Experiment - Progress Report*. Tech. rep. CERN-SPSC-2019-010. SPSC-SR-248. Geneva: CERN, Jan. 2019. URL: <https://cds.cern.ch/record/2654870>.
- [14] P.A. Zyla et al. (Particle Data Group). “Tau - Particle Data Group”. In: (2020). URL: <https://pdg.lbl.gov/2020/listings/rpp2020-list-tau.pdf>.
- [15] C. Ahdida et al. *SHiP Experiment - Comprehensive Design Study report*. Tech. rep. CERN-SPSC-2019-049. SPSC-SR-263. Geneva: CERN, Dec. 2019. URL: <https://cds.cern.ch/record/2704147>.
- [16] Wikipedia. *Schematic of a photomultiplier tube*. URL: https://en.wikipedia.org/wiki/Photomultiplier_tube#/media/File:PhotoMultiplierTubeAndScintillator.svg (visited on 12/20/2020).
- [17] Walter Blum, Werner Riegler, and Luigi Rolandi. *Particle detection with drift chambers*. Springer Science & Business Media, 2008.
- [18] Christian Felix Hermanns. “X-ray absorption studies of metalloporphyrin molecules on surfaces: Electronic interactions, magnetic coupling, and chemical switches”. PhD thesis. 2013.

- [19] Stefan Bieschke. “Examination of different drift gas mixtures for the muon magnetic spectrometer for the SHiP experiment”. Universität Hamburg, 2016.
- [20] Torben Ferber. “Messung der Gaseigenschaften unter Einfluss von molekularem Sauerstoff und Aufbau eines Gassystems für das Driftröhren–Myon–Spektrometer des OPERA–Detektors”. Universität Hamburg, 2006.
- [21] Ekbert Hering, Klaus Bressler, and Jürgen Gutekunst. *Elektronik für Ingenieure und Naturwissenschaftler*. Springer-Verlag, 2008.
- [22] N. Agafonova et al. “Final Results of the OPERA Experiment on ν_τ Appearance in the CNGS Neutrino Beam”. In: *Phys. Rev. Lett.* 120 (21 May 2018), p. 211801. DOI: 10.1103/PhysRevLett.120.211801. URL: <https://link.aps.org/doi/10.1103/PhysRevLett.120.211801>.
- [23] R. Zimmermann et al. “The precision tracker of the OPERA detector”. In: *Nuclear Instruments and Methods in Physics Research Section A: Accelerators, Spectrometers, Detectors and Associated Equipment* 555.1 (2005), pp. 435–450. ISSN: 0168-9002. DOI: <https://doi.org/10.1016/j.nima.2005.09.003>. URL: <http://www.sciencedirect.com/science/article/pii/S0168900205018061>.
- [24] Benedict Kaiser. “Setup of a prototype for the SHiP Spectrometer Straw Tracker”. Universität Hamburg, 2019.
- [25] Felix Bergholz. “Aufbau und Inbetriebnahme eines Teststandes zur Charakterisierung von Strawtubes bei unterschiedlichen Betriebsspannungen”. Universität Hamburg, 2020.
- [26] Jan Sewing. “Entwicklung und Bestimmung der Nachweiseigenschaften des Myon-Detektors für das OPERA-Experiment”. Universität Hamburg, 2006.
- [27] William R Leo. *Techniques for nuclear and particle physics experiments: a how-to approach*. Springer Science & Business Media, 2012.
- [28] Werner Riegler. “Limits to Drift chamber resolution”. PhD thesis. Vienna, Tech. U., 1998.
- [29] R. Brun and F. Rademakers. “ROOT: An object oriented data analysis framework”. In: *Nucl. Instrum. Meth. A* 389 (1997). Ed. by M. Werlen and D. Perret-Gallix, pp. 81–86. DOI: 10.1016/S0168-9002(97)00048-X.
- [30] Detlef Bartsch. *Energy-loss measurement with the ZEUS Central Tracking Detector*. Tech. rep. Bonn Univ.(Germany). Physikalisches Inst., 2007.

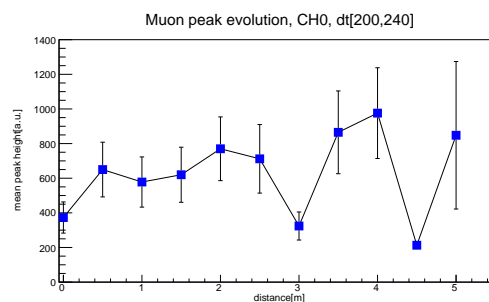
Appendix A

Additional Figures

A graph was created for each channel for all measurement series. Since 24 plots alone for the muon measurement series is too much even for the appendix, only a selection of plots is shown here. The figures A.1, A.2 and A.3 are additional plots for the muon measurement series. Figure A.4 depicts additional plots of the measurements series for gamma signals. figure A.5 visualizes the mean pulse shape of gamma signals for channel 1 and 2.

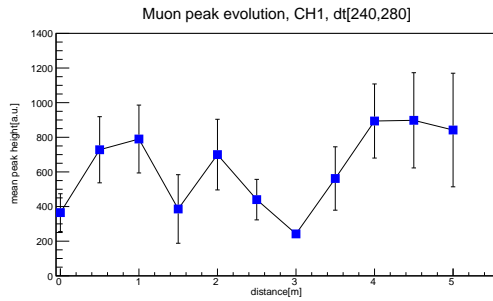


(a) Channel 1, drift times used in the range of 160 - 200

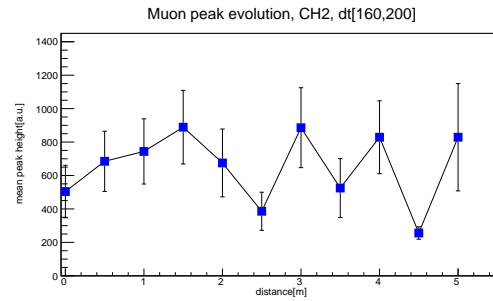


(b) Channel 3, drift times used in the range of 200 - 240

Figure A.1: Signal height evolution for muon events. Here visualized for channel 0 and 1, with the HV set to 1900 V/ 2100 V.

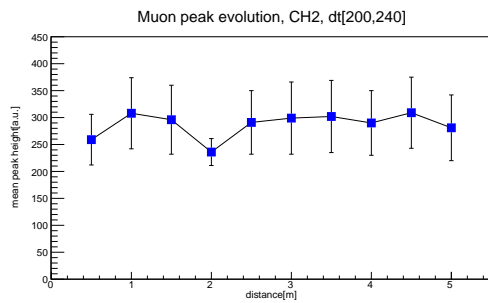


(a) Channel 1, drift times used in the range of 240 - 280

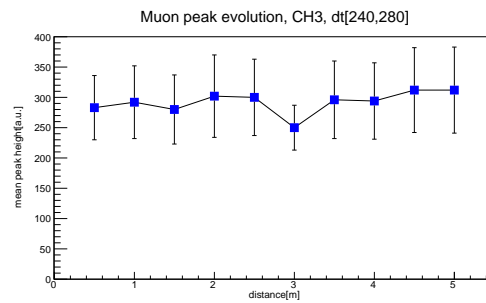


(b) Channel 2, drift times used in the range of 160 - 200

Figure A.2: Signal height evolution for muon events. Here visualized for channel 1 and 2, with the HV set to 1900 V/ 2100 V.

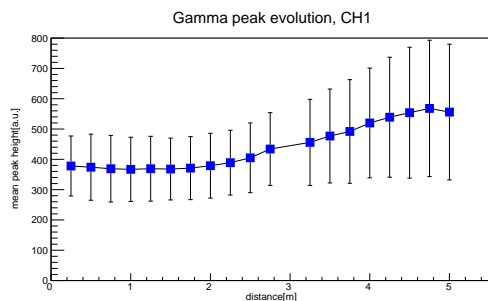


(a) Channel 2, drift times used in the range of 200 - 240

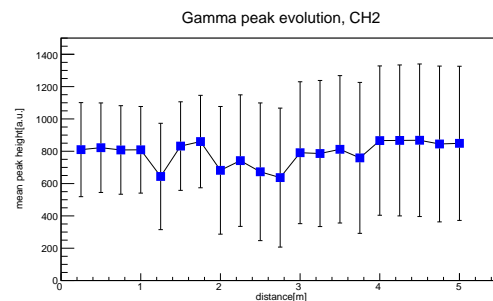


(b) Channel 2, drift times used in the range of 240 - 280

Figure A.3: Signal height evolution for muon events. Here visualized for channel 2, with the HV set to 1800 V/ 2000 V.



(a) Channel 1, with a HV of 1800 V/ 2000 V



(b) Channel 2, with a HV of 1900 V/ 2100 V

Figure A.4: Signal height evolution for gamma events. Here visualized for channel 1, with the HV set to 1800 V/ 2000 V and for channel 2, with the HV set to 1900 V/ 2100 V.

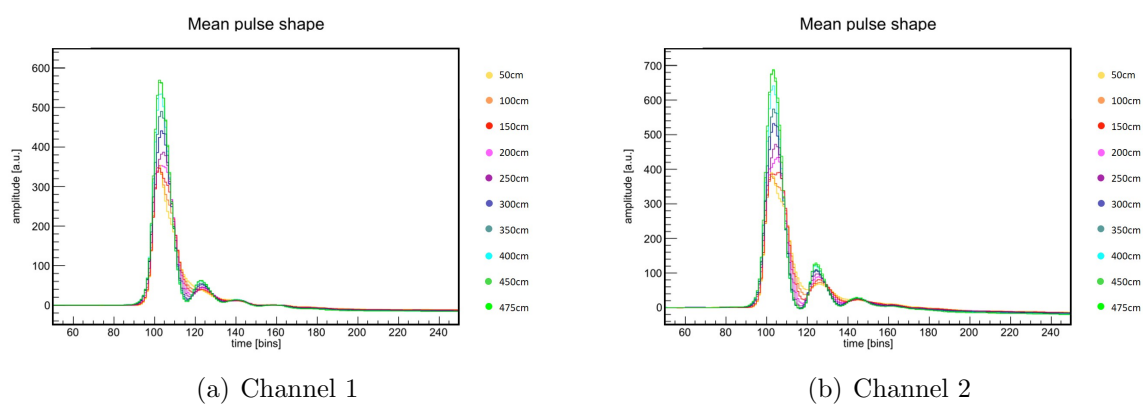


Figure A.5: Evolution of the pulse shape for gamma events. Here visualized for channel 1 and 2, with the HV set to 1900 V/ 2100 V.

